

Supporting Information

Band Engineering of Multicomponent Semiconductors: A General Theoretical Model on the Anion Group

X. Y. Meng ^{§, *, 1}, D. Y. Liu ^{§, 1}, G. W. Qin ^{*, 2}

¹College of Sciences; ²Key Laboratory for Anisotropy and Texture of Materials (Ministry of Education), School of Materials Science and Engineering, Northeastern University, Shenyang 110819, China

1. Calculation method

1.1 ABO_3 perovskite semiconductors

The geometry optimization and the electronic structure calculations of all perovskites were performed using the Vienna ab initio simulation package (VASP) code based on density functional theory (DFT).¹⁻⁴ The kinetic-energy cutoff in the expansion of the electronic wave function was set to of 600 eV and Brillouin zone was sampled with a (18×18×18) Monkhorst–Pack k-point mesh.⁵ The electronic structures were evaluated with HSE exchange-correlation functional.⁶ For the bulk geometry optimization, the absolute convergence of the total energy with respect to the structural degrees of freedom was less than 1meV/atom. In this work, the absolute energy (relative to the vacuum) of edges of conduction and valence bands (CBM and VBM) is determined by the surface method within the same DFT framework as our previous work.⁷

1.2 $\text{Zn}_x\text{Mg}_{(1-x)}\text{Fe}_2\text{O}_4$ spinel semiconductors

As D. A. Andersson *et al.* pointed out that the conventional cell containing 56 atoms is sufficient to imitate the spinels,⁸ we selected MgFe_2O_4 normal spinel conventional cell (space group: Fd-3mz) as the initio structure in which total 56 atoms were filled. There are 8 A-site Mg atoms and 16 B-site Fe atoms in the cell.⁹ Then the A-site Mg atoms was partially replaced by Zn atoms according to the component ratio x to get the model of $\text{Zn}_x\text{Mg}_{(1-x)}\text{Fe}_2\text{O}_4$ (x from 0 to 1 at an interval of 0.125) solid solutions. In order to characterize the random feature of the solid solution phases,

the special quasi-random structures (SQSs) based on the normal spinel lattice at different x values are generated by Alloy-Theoretic Automated Toolkit (ATAT) package.^{10, 11} Among available SQS models for $Zn_xMg_{(1-x)}Fe_2O_4$, the cell with the lowest total energy is picked up as the equilibrium structure at each x value.

All the total energy and geometry optimization calculations are carried out by VASP in the framework of DFT.¹⁻⁴ The electron structure calculations were performed with the self-consistent spin-polarized methods. The Perdew-Burke-Ernzerhof (PBE)¹² pseudopotential was chosen as the exchange and correlation functional. $3s^2$, $3d^{10}4s^2$, $3d^64s^2$, and $2s^22p^4$ orbitals were treated as valence electronic states for Mg, Zn, Fe, and O elements, respectively. An expansion of the electronic wave functions in plane waves with a kinetic-energy cutoff of 600 eV was adopted. Brillouin-zone integration was performed using a $6\times 6\times 6$ Monkhorst-Pack k -point mesh,⁵ and the convergence criteria for the total energy and Hellmann-Feynman force was set to 10^{-6} eV and 1 meV/ \AA , respectively. Due to the strong on-site Coulomb repulsion between the localized d-shell electrons, the Hubbard U term was added to the potential of Fe and the value of U was set to 4.5 eV.^{13, 14}

As for the band edges, using the slab model, the absolute position of VBM/CBM at PBE+U level is computed with the equation:¹⁵

$$E_{\text{CBM/VBM}}^{\text{PBE+U}} = \Delta\bar{V}_{\text{bulk-vac}} - \bar{V}_{\text{bulk}} + (E_{\text{BGC}} \pm \frac{1}{2}\Delta E_g^{\text{PBE+U}}) \quad (\text{S1})$$

Where $\Delta\bar{V}_{\text{bulk-vac}}$ is the average electrostatic potential in the bulk region of the slab relative to the vacuum region.¹⁶ The slab should be sufficiently thick to mimic the bulk of the material, and the vacuum region should be large enough to avoid the interaction with the neighboring replica. \bar{V}_{bulk} is the bulk electrostatic potential averaged over the plane parallel to the specific surface of bulk semiconductors. EBGC is the band gap center position. According to Perdew and Levy, DFT is exact for calculating the band gap center (EBGC).¹⁷ Therefore we adopt PBE functional to calculate the bulk band gap center. Hubbard U-correction for bulk VBM (CBM) is made by subtracting (adding) the half of PBE+U gap.

2. Ground state and stability of $Zn_xMg_{(1-x)}Fe_2O_4$

To verify the equilibrium structure of normal the relation between the total energy and volume was checked. We found that the Mg-O and Zn-O bond become shorter with the increase of Zn .at%, indicating the larger electronegativity of Zn. The calculated curves of the equation of state (EOS) for normal spinel $ZnFe_2O_4$ and $MgFe_2O_4$ in non-magnetic (NM), ferromagnetic (FM) and anti-ferromagnetic (AFM) phases are shown in Fig. S3. Obviously, NM- $MgFe_2O_4$ and NM- $ZnFe_2O_4$ are less stable compared to FM and AFM phases at ambient conditions. Although the energy difference is slight, it turns out that the stability of AFM phase is superior to that of FM phase (see Fig. S3), which is consistent with the report of S. Soliman and Q. Chen.^{18, 19}

Based on the AFM ground state, we determined the equilibrium configuration among all available SQS solid solution models by the total energy calculations. As is shown in Table S5, the optimized equilibrium lattice parameter and lattice volume of $Zn_xMg_{(1-x)}Fe_2O_4$ decrease gradually with the increase of Zn content due to its relative smaller ionic radius.

To study the thermodynamic stability and miscibility of $Zn_xMg_{(1-x)}Fe_2O_4$ at each x value, the formation enthalpy ($E_{formation}$) and mixing energy (E_{mixing}) were calculated. As a function of compositions, $E_{formation}$ is defined as the following equation.²⁰

$$E_{formation}^{(x)} = \frac{E_{total}^{(x)} - xE_{solid}^{Zn} - (1-x)E_{solid}^{Mg} - 2E_{solid}^{Fe} - 4E_{gas}^{O_2}}{7} \quad (S2)$$

Where $E_{total}^{(x)}$ is the total energy of $Zn_xMg_{(1-x)}Fe_2O_4$ at a specified x . E_{solid}^{Mg} or E_{solid}^{Zn} is the energy of single Mg or Zn atom in its elemental state, and $E_{gas}^{O_2}$ is the half of the energy of oxygen gas. From Fig. S4 and Table S5, it is found that all the formation enthalpies of equilibrium SQS configurations are negative, which indicates that the normal spinels $Zn_xMg_{(1-x)}Fe_2O_4$ are thermodynamically stable.

E_{mixing} of solutions with respect to $ZnFe_2O_4$ and $MgFe_2O_4$ is determined by eqn (S3):²¹

$$E_{mixing}^{(x)} = \frac{E_{total}^{(x)} - xE_{total}^{ZnFe_2O_4} - (1-x)E_{total}^{MgFe_2O_4}}{7} \quad (S3)$$

Here $E_{total}^{ZnFe_2O_4}$ and $E_{total}^{MgFe_2O_4}$ stands for the total energy of $ZnFe_2O_4$ and $MgFe_2O_4$, respectively.

Generally speaking, the negative mixing energy is contributed to the formation of stable solutions, while the positive value suggests a tendency for the phase separation. In Fig. S5, the curve of negative mixing energies of $Zn_xMg_{(1-x)}Fe_2O_4$ show a parabolic concave with a minimum at $x = 0.5$ (Table S5). Thus our calculations suggest that $Zn_xMg_{(1-x)}Fe_2O_4$ are continuous solid solutions from $x = 0$ to 1 at 0 K owing to the small size-mismatch (less than 0.1%) between $MgFe_2O_4$ and $ZnFe_2O_4$ lattices. At elevated temperatures, the effect of the mixing entropy may further stabilize these solid solutions. So far our thermodynamic calculations confirm the ground states $Zn_xMg_{(1-x)}Fe_2O_4$ at each x and support that the $Zn_xMg_{(1-x)}Fe_2O_4$ continuous solid solutions are stable and can be experimentally synthesized.

3. Supporting for the general anion group model

The reported values of band gaps of a series of MCSCs (as shown in Tab. S6 and Fig. S6-S10) are well consistent with the predictions of the anion group model, which further confirms the validity of the anion group model.

Table S1. Optimized lattice constants a (Å), band gaps E_g (eV) and CBM positions E_c (eV) for cubic titanates and zirconates.

Anion group	Compounds	a	$a^{(\text{Exp.})}$	$E_g^{(\text{HSE})}$	$E_g^{(\text{Exp.})}$	$E_g^{(\text{Cal.})}$	E_c	$E_c^{(\text{Ref.})}$
(TiO_6)	CaTiO_3	3.89	3.85 ²²	3.35	3.50 ²³	3.25 ²⁴	-2.54	-3.58 ²⁵
	SrTiO_3	3.94	3.87 ²⁶	3.34	3.40 ²⁷	3.20 ²⁸	-3.03	-3.70 ²⁹
	BaTiO_3	4.03	3.99 ³⁰	3.04	3.30 ²⁷	3.18 ³¹	-4.06	-4.58 ²⁷
(ZrO_6)	CaZrO_3	4.16	4.02 ³²	4.80	5.70 ³³	3.40 ³⁴	-1.83	-2.49 ³³
	SrZrO_3	4.20	4.10 ³⁵	4.79	5.50 ²⁸	3.34 ³⁶	-2.17	-2.67 ³⁷
	BaZrO_3	4.26	4.19 ³⁸	4.56	5.30 ³⁹	3.23 ³⁶	-2.28	-2.70 ⁴⁰

Table S2. The band gap E_g (eV) and CBM position E_c (eV) for the selected perovskite-type niobates.

Anion group	Compounds	$E_g^{(\text{HSE})}$	E_c	$E_g^{(\text{Ref.})}$	$E_c^{(\text{Ref.})}$
(NbO_6)	NaNbO_3	3.11	-2.12	3.44 ⁴¹	-3.28 ⁴²
	KNbO_3	2.67	-2.83	3.30 ⁴³	-3.64 ²⁷

Table S3. The band gap E_g (eV) and CBM position E_c (eV) for the selected perovskite-type stannates.

Anion group	Compounds	$E_g^{(\text{HSE})}$	E_c	$E_g^{(\text{Ref.})}$	$E_c^{(\text{Ref.})}$
	CaSnO_3	3.07	-2.51	4.40 ⁴⁴	-3.04 ⁴⁵
(SnO_6)	SrSnO_3	2.67	-2.92	3.90 ⁴⁶	-3.13 ⁴⁵
	BaSnO_3	2.04	-3.56	3.10 ⁴⁷	-3.81 ⁴⁵

Table S4. The ionicity of different 'B' site cations in titanates, zirconates, niobates, and stannates.

'B' cations	iconicity
Ti^{4+}	57.5%
Zr^{4+}	60.0%
Nb^{5+}	50.0%
Sn^{4+}	~100%

Table S5. The calculated lattice parameters a (\AA), equilibrium volume V ($\text{\AA}^3/\text{unit cell}$), average bond length for Zn-O, Mg-O, and Fe-O (\AA), formation energy $E_{formation}$ ($eV/atom$), and mixing energy E_{mixing} ($meV/atom$) for $\text{Zn}_x\text{Mg}_{(1-x)}\text{Fe}_2\text{O}_4$ (x from 0 to 1 at an interval of 0.125).

x	a	V	Mg-O	Zn-O	Fe-O	$E_{formation}$	E_{mixing}
0	8.5057	615.34	1.9952	×	2.0416	-1.54	0
0.125	8.5062	615.46	1.9961	1.9992	2.0411	-1.50	-0.29
0.250	8.5065	615.53	1.9968	2.0003	2.0406	-1.45	-0.57
0.375	8.5069	615.60	1.9969	2.0018	2.0401	-1.40	-1.05
0.500	8.5071	615.65	1.9969	2.0031	2.0396	-1.36	-1.34
0.625	8.5075	615.75	1.9983	2.0026	2.0392	-1.31	-1.09
0.750	8.5076	615.78	1.9996	2.0028	2.0387	-1.26	-0.68
0.825	8.5078	615.81	2.0011	2.0032	2.0383	-1.21	-0.43
1.000	8.5078	615.81	×	2.0038	2.0378	-1.17	0

Table S6. Band gaps of AB₂O₄ spinels, including both calculations and available experiments.

(eV)	Mg			Ca			Sr			Ba			Mn			Fe		
	PBE	HSE	EXP	PBE	HSE	EXP	PBE	HSE	EXP	PBE	HSE	EXP	PBE	HSE	EXP	PBE	HSE	EXP
Cr	0	4.23	0.69	0	4.38	2.4	0	4.33		0	4.12	1.6	0	3.7		0	0	1.33
Fe	0	2.95	2.08	0	2.90		0	2.87		0	2.67		0	0.89		0	0	
Co	1.03	3.96		1.11	3.96		1.02	3.77		0.96	3.44		0	2.45	2.11	0		
Ni	0	0		0	0		0	0		0	0		0	0		0	0	
Al	5.71	6.93	7.8	4.06	5.75		3.16	4.81		2.36	3.93		0	4.52	4.1	0	0	2.7
Ga	3.14	4.82		2.67	4.29		1.99	3.58		1.36	2.87		0	2.63		0	0	
In	1.85	3.35	3.4	2.01	3.41		1.81	3.18		1.51	2.92		0	2.16		0	0	

(eV)	Co			Ni			Cu			Zn			Cd			Pd		
	PBE	HSE	EXP	PBE	HSE	EXP	PBE	HSE	EXP	PBE	HSE	EXP	PBE	HSE	EXP	PBE	HSE	EXP
Cr	0	3.67	1.61 ⁹	0			0	0	1.4 ¹⁰	0	4.05		0	3.91		0	0	
Fe	0	1.21	0.6 ¹¹	0	0	1.7 ¹²	0	0	1.48 ¹³	0	2.75	1.93 ¹⁴	0	2.91		0	0.54	
Co	0	2.98		0	0		0	0		0.90	3.77	2.8 ¹⁵	0.82	3.52		0	0	
Ni	0	0		0			0	0		0	0		0	0		0	0	
Al	0	4.97	2.3 ¹⁶	0	0	2.85 ¹⁷	0	0	1.77 ¹⁸	3.85	5.70	3.9 ¹⁹	2.69	4.31		0	0.47	
Ga	0	3.16		0	0		0	0		2.37	4.05	4.4 ¹⁹	1.67	3.14	3.5 ²⁰	0	0	
In	0	1.48		0	0		0	0		1.18	2.73		0.91	2.36	2.23 ²¹	0	0	

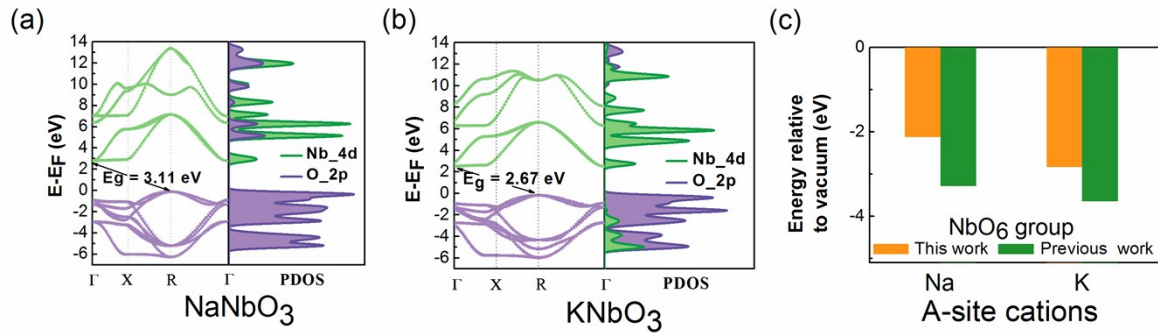


Fig. S1 (a) HSE band structures and PDOS of ANbO₃ (A = Na, K). The Fermi level is set to zero. (b) The CBM positions for ANbO₃ (A = Na, K). The experimental values can be found in: Ref. 42 for NaNbO₃ and Ref. 27 for KNbO₃.

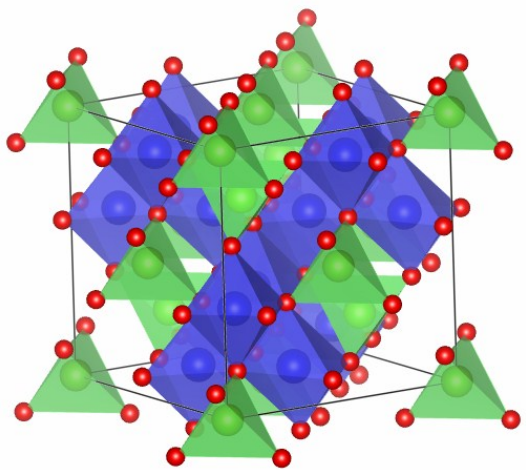


Fig. S2 The prototype model for the AB_2O_4 normal spinel structure containing 56 atoms. Color code: green A-site atoms; blue B-site atoms; and red O atoms.

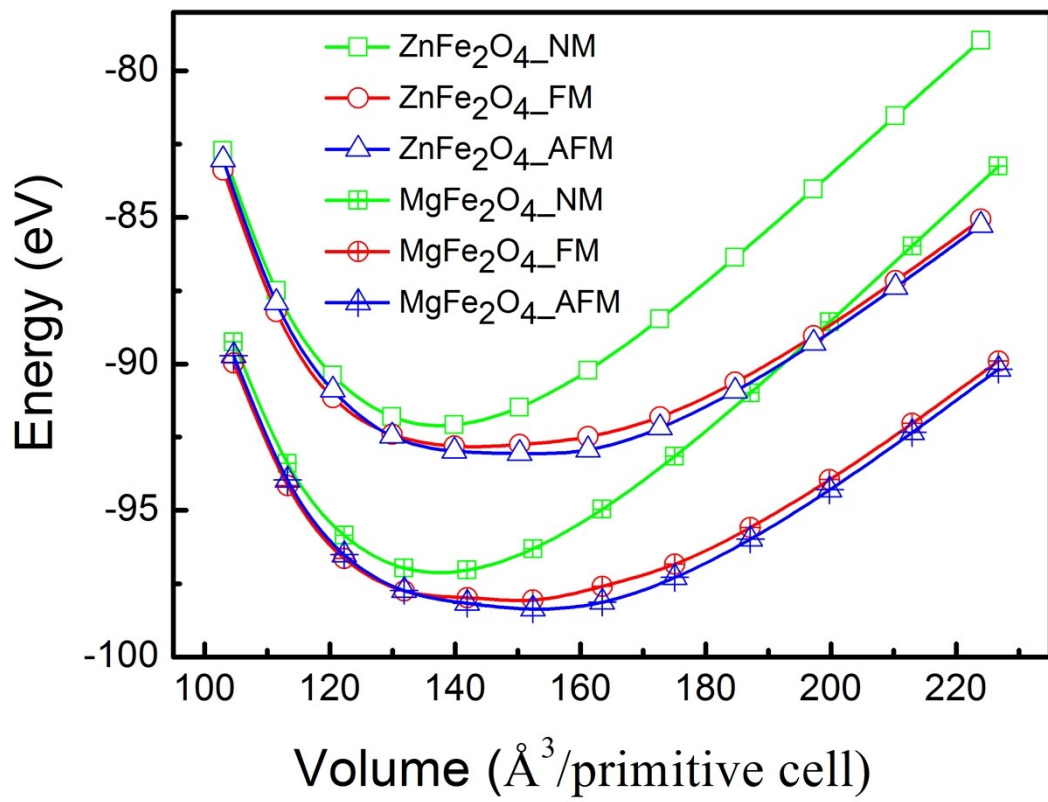


Fig. S3 The calculated EOS curves for MgFe_2O_4 and ZnFe_2O_4 of different magnetic configurations.

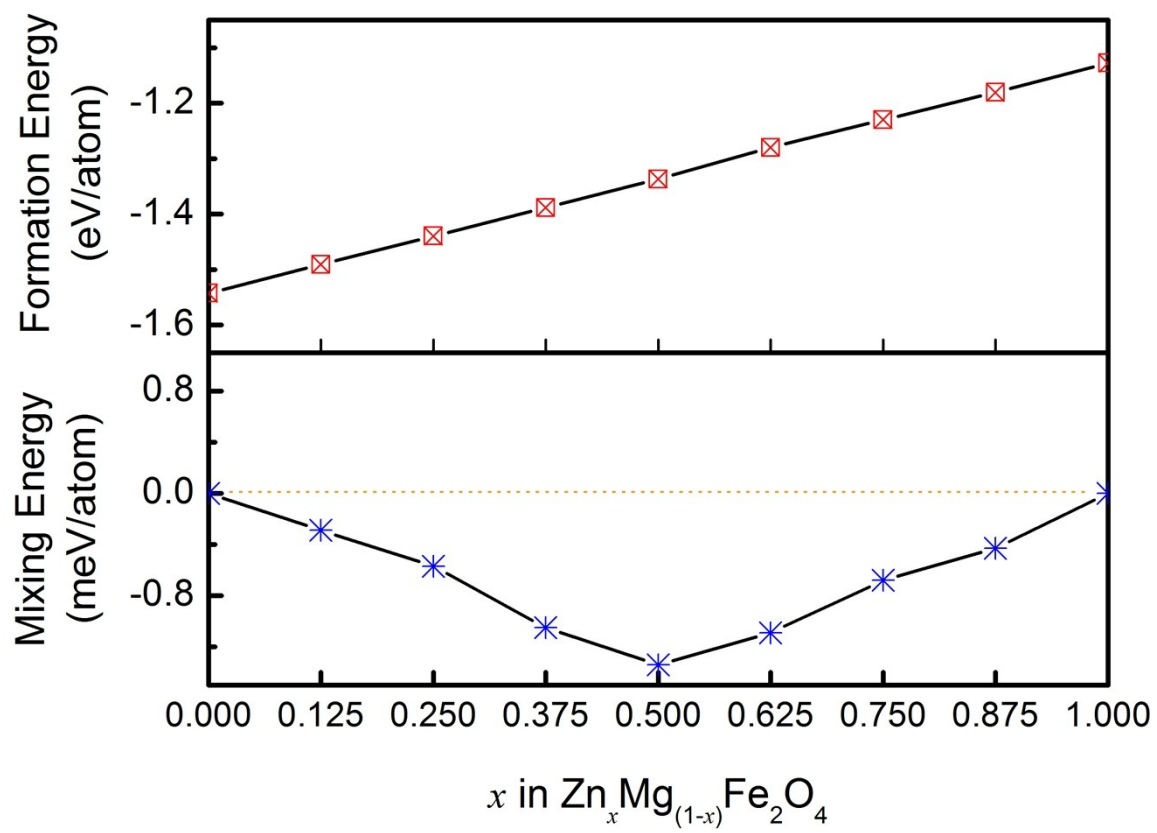


Fig. S4 DFT calculated formation energy $E_{formation}$ and mixing energy E_{mixing} for $\text{Zn}_x\text{Mg}_{(1-x)}\text{Fe}_2\text{O}_4$ (x from 0 to 1 at an interval of 0.125).

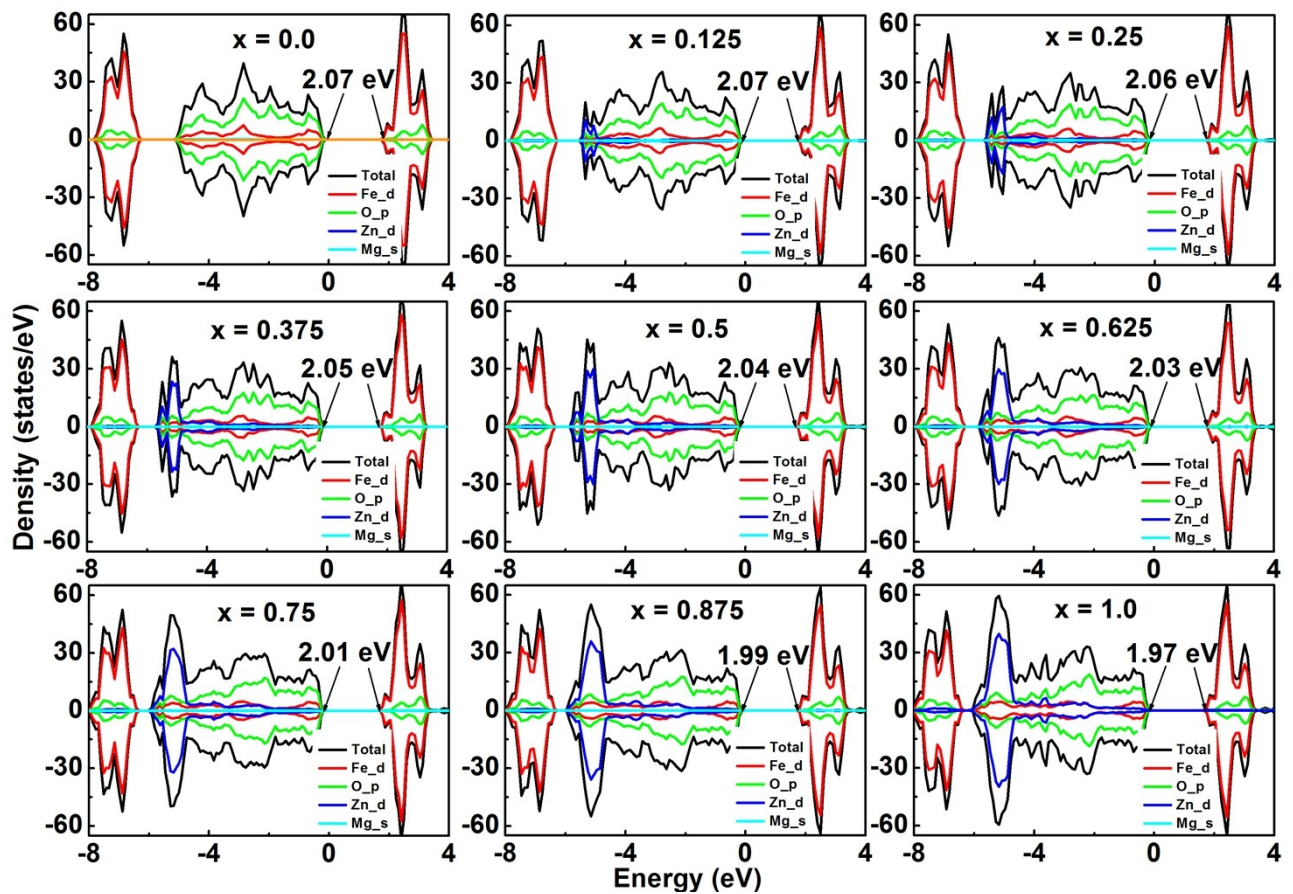


Fig. S5 DFT+U calculated PDOS for $Zn_xMg_{(1-x)}Fe_2O_4$ (x from 0 to 1 at an interval of 0.125).

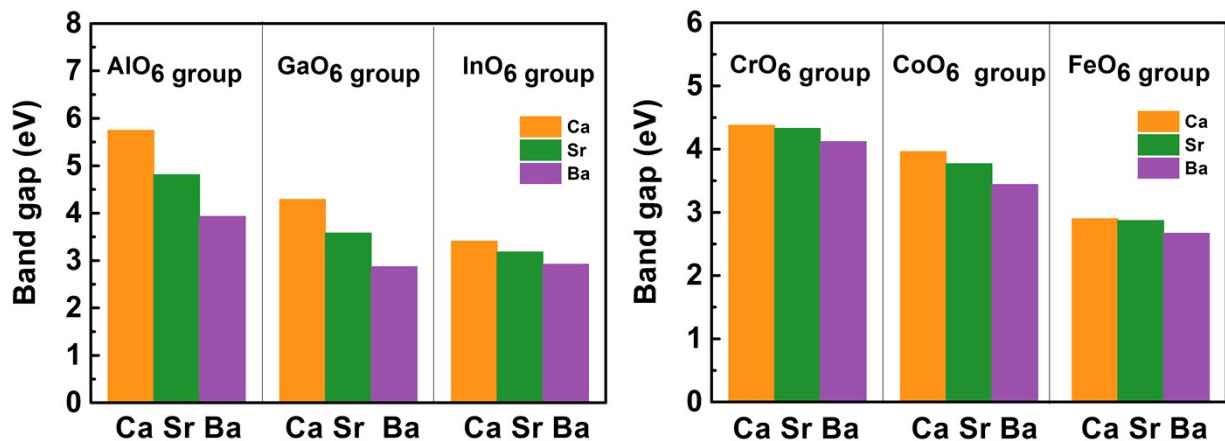


Fig. S6 HSE calculated band gap for AB_2O_4 ($\text{A} = \text{Ca}, \text{Sr}, \text{Ba}; \text{B} = \text{Al}, \text{Ga}, \text{In}, \text{Cr}, \text{Co}, \text{Fe}$).

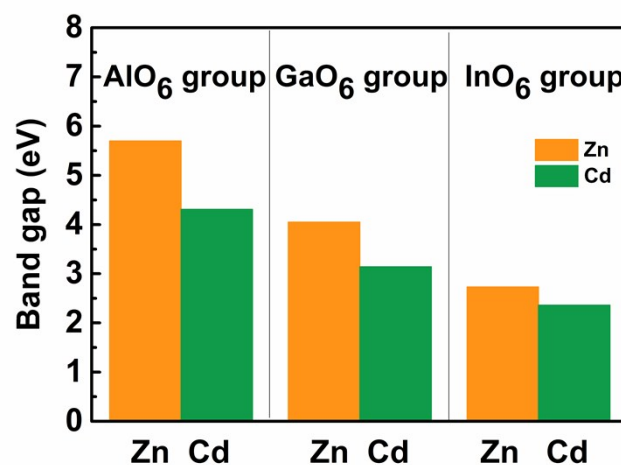


Fig. S7 HSE calculated band gap for AB_2O_4 ($\text{A} = \text{Zn}, \text{Cd}; \text{B} = \text{Al}, \text{Ga}, \text{In}$).

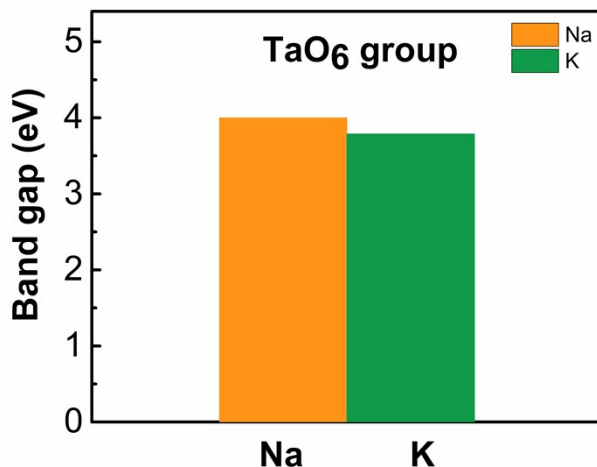


Fig. S8 Band gap of ATaO₃ (A = Na, K). The reported experimental gaps can be found in: Ref. 48 for NaTaO₃; Ref. 49 for KTaO₃.

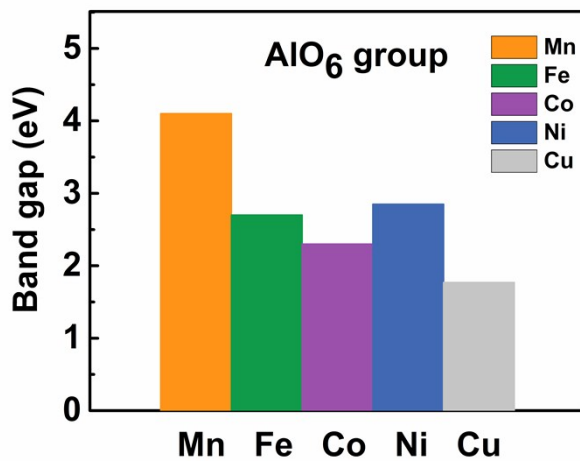


Fig. S9 Band gaps of AAl₂O₄ (A = Mn, Fe, Co, Ni, Cu). The reported experimental gaps can be found in: Ref. 50 for MnAl₂O₄; Ref. 51 for FeAl₂O₄; Ref. 52 for CoAl₂O₄; Ref. 53 for NiAl₂O₄; Ref. 54 for CuAl₂O₄.

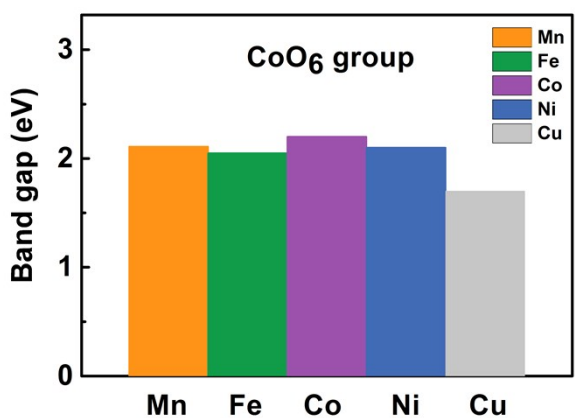


Fig. S10 Band gaps of AB₂O₄ (A = Mn, Fe, Co, Ni, Cu; B = Co). The reported experimental gaps can be found in: Ref. 55 for MnCo₂O₄; Ref. 56 for FeCo₂O₄; Ref. 57 for Co₃O₄; Ref. 57 for NiCo₂O₄; Ref. 58 for CuCo₂O₄.

Reference

- 1 G. Kresse and J. Hafner, *Phys. Rev. B*, 1993, **48**, 13115.
- 2 G. Kresse and J. Furthmüller, *Phys. Rev. B*, 1996, **54**, 11169.
- 3 G. Kresse and J. Furthmüller, *Comp. Mater. Sci.*, 1996, **6**, 15-50.
- 4 W. Kohn and L. J. Sham, *Phys. Rev.*, 1965, **140**, A1133.
- 5 H. J. Monkhorst, J. D. Pack, *Phys. Rev. B*, 1976, **13**, 5188.
- 6 J. Heyd, G. E. Scuseria and M. Ernzerhof, *J. Chem. Phys.*, 2003, **118**, 8207-8215.
- 7 X. Meng, L. Wang, D. Liu, X. Wen, Q. Zhu, W. A. Goddard III and Q. An, *Chem. Mater.*, 2016, **28**, 1335-1342.
- 8 D. A. Andersson and C. R. Stanek, *Phys. Chem. Chem. Phys.*, 2013, **15**, 15550-15564.
- 9 D. M. Wells, J. Cheng, D. E. Ellis and B. Wessels, *Phys. Rev. B*, 2010, **81**, 174422.
- 10 S.-H. Wei, L. Ferreira, J. E. Bernard and A. Zunger, *Phys. Rev. B*, 1990, **42**, 9622.
- 11 A. Van De Walle, M. Asta and G. Ceder, *Calphad*, 2002, **26**, 539-553.
- 12 J. P. Perdew, K. Burke and M. Ernzerhof, *Phys. Rev. Lett.*, 1996, **77**, 3865.
- 13 N. J. Mosey, P. Liao and E. A. Carter, *J. Chem. Phys.*, 2008, **129**, 014103.
- 14 V. Antonov, B. Harmon and A. Yaresko, *Phys. Rev. B*, 2003, **67**, 024417.
- 15 Y. Ping, D. Rocca and G. Galli, *Chem. Soc. Rev.*, 2013, **42**, 2437-2469.
- 16 T. Jing, Y. Dai, X. Ma, W. Wei and B. Huang, *J. Phys. Chem. C*, 2015, **119**, 27900-27908.
- 17 J. P. Perdew and M. Levy, *Phys. Rev. Lett.*, 1983, **51**, 1884.
- 18 S. Soliman, A. Elfalaky, G. H. Fecher and C. Felser, *Phys. Rev. B*, 2011, **83**, 085205.
- 19 Q. Chen and Z. J. Zhang, *Appl. Phys. Lett.*, 1998, **73**, 3156.
- 20 X.-J. Chen, M.-X. Zeng, R.-N. Wang, Z.-S. Mo, B.-Y. Tang, L.-M. Peng and W.-J. Ding, *Comp. Mater. Sci.*, 2012, **54**, 287-292.

- 21 Y. Wu and G. Ceder, *J. Phys. Chem. C*, 2013, **117**, 24710-24715.
- 22 C.-J. Eklund, C. Fennie and K. Rabe, *Phys. Rev. B*, 2009, **79**, 220101.
- 23 K. Ueda, H. Yanagi, R. Noshiro, H. Hosono and H. Kawazoe, *J. Phys.: Condens. Matter*, 1998, **10**, 3669.
- 24 K. Van Benthem, C. Elsässer and R. French, *J. Appl. Phys.*, 2001, **90**, 6156-6164.
- 25 Y. Wang, C.-G. Niu, L. Wang, Y. Wang, X.-G. Zhang and G.-M. Zeng, *Rsc Adv.*, 2016, **6**, 47873-47882.
- 26 L. M. Liborio, C. G. Sánchez, A. T. Paxton and M. W. Finnis, *J. Phys.: Condens. Matter*, 2005, **17**, L223.
- 27 Y. S. Xu and M. A. A. Schoonen, *Am. Mineral.*, 2000, **85**, 543-556.
- 28 J. Robertson, K. Xiong and S. Clark, *Thin Solid Films*, 2006, **496**, 1-7.
- 29 B. Modak, K. Srinivasu and S. K. Ghosh, *Phys. Chem. Chem. Phys.*, 2014, **16**, 24527-24535.
- 30 K. Rushchanskii, S. Kamba, V. Goian, P. Vaněk, M. Savinov, J. Prokleška, D. Nuzhnny, K. Knížek, F. Laufek and S. Eckel, *Nat. Mater.*, 2010, **9**, 649.
- 31 S. Piskunov, E. Kotomin, E. Heifets, J. Maier, R. Egglitis and G. Borstel, *Surf. Sci.*, 2005, **575**, 75-88.
- 32 R. W. G. Wyckoff, *Crystal structures*, Interscience, New York, 1960.
- 33 I. L. V. Rosa, M. Oliveira, M. Assis, M. Ferrer, R. André, E. Longo and M. F. Gurgel, *Ceram. Int.*, 2015, **41**, 3069-3074.
- 34 P. Stoch, J. Szczerba, J. Lis, D. Madej and Z. Pędziuch, *J. Eur. Ceram. Soc.*, 2012, **32**, 665-670.
- 35 B. J. Kennedy, C. J. Howard and B. C. Chakoumakos, *Phys. Rev. B*, 1999, **59**, 4023.
- 36 R. Terki, H. Feraoun, G. Bertrand and H. Aourag, *Phys. Status Solidi B*, 2005, **242**, 1054-1062.
- 37 Z. Guo, B. Sa, B. Pathak, J. Zhou, R. Ahuja and Z. Sun, *Int. J. Hydrogen Energy*, 2014, **39**,

2042-2048.

- 38 S. Yamanaka, M. Fujikane, T. Hamaguchi, H. Muta, T. Oyama, T. Matsuda, S.-i. Kobayashi and K. Kurosaki, *J. Alloys Compd.*, 2003, **359**, 109-113.
- 39 J. Robertson, *J. Vac. Sci. Technol. B*, 2000, **18**, 1785-1791.
- 40 Y. Yuan, X. Zhang, L. Liu, X. Jiang, J. Lv, Z. Li and Z. Zou, *Int. J. Hydrogen Energy*, 2008, **33**, 5941-5946.
- 41 J. Kubacki, A. Molak and E. Talik, *J. Alloys Compd.*, 2001, **328**, 156-161.
- 42 Q. Gu, K. Zhu, N. Zhang, Q. Sun, P. Liu, J. Liu, J. Wang and Z. Li, *J. Phys. Chem. C*, 2015, **119**, 25956-25964.
- 43 F. Wang and A. M. Rappe, *Phys. Rev. B*, 2015, **91**, 165124.
- 44 X. Fan, W. Zheng, X. Chen and D. J. Singh, *PLoS ONE*, 2014, **9**, e91423.
- 45 W. Zhang, J. Tang and J. Ye, *J. Mater. Res.*, 2007, **22**, 1859-1871.
- 46 B. Bellal, B. Hadjarab, A. Bouguelia and M. Trari, *Theor. Exp. Chem.*, 2009, **45**, 172-179.
- 47 H. Mizoguchi, H. W. Eng and P. M. Woodward, *Inorg. Chem.*, 2004, **43**, 1667-1680.
- 48 J. Xu, D. Xue and C. Yan, *Mater. Lett.*, 2005, **59**, 2920-2922.
- 49 S. Cabuk, H. Akkus and A.M. Mamedov, *Physica B*, 2007, **394**, 81–85.
- 50 U. Hålenius, F. Bosi and H. Skogby, *Am. Mineral.*, 2007, **92**, 1225-1231.
- 51 U. Hålenius, H. Skogby and G. B. Andreozzi, *Phys. Chem. Miner.*, 2002, **29**, 319-330.
- 52 U. L. Štangar, B. Orel and M. Krajnc, *J. Sol-Gel Sci. Technol.* 2003, **26**, 771-775.
- 53 M. Maddahfar, M. Ramezani, M. Sadeghi and A. Sobhani-Nasab, *J. Mater. Sci.: Mater. Electron.*, 2015, **26**, 7745-7750.
- 54 L. C. Leu, D. P. Norton, G. E. Jellison, V. Selvamanickam and X. Xiong, *Thin Solid Films*, 2007, **515**, 6938-6942.

55 S. M. A. Shibli, P. S. Arun and A. V. Raj, *RSC Adv.*, 2015, **5**, 19393–19399.

56 D. Zhang, G. Zhang and L. Zhang, *Chem. Eng. J.*, 2017, **330**, 792–803.

57 M. Liu, L. Kong, C. Lu, X. Li, Y. Luo, and L. Kang, *ACS Appl. Mater. Interfaces*, 2012, **4**, 4631–4636.

58 K. T. Alali, Z. Lu, H. Zhang, J. Liu, Q. Liu, R. Li, K. Aljebawi and J. Wang, *Inorg. Chem. Front.*, 2017, **4**, 1219–1230.